CHALMERS |  UNIVERSITY OF GOTHENBURG

PREPRINT 2010:33

Model adaptivity for plates based on a continuous-discontinuous finite element method

DAVID HEINTZ

Department of Mathematical Sciences
Division of Mathematics
CHALMERS UNIVERSITY OF TECHNOLOGY
UNIVERSITY OF GOTHENBURG
Gothenburg Sweden 2010

Preprint 2010:33

Model adaptivity for plates based on a continuous-discontinuous finite element method

David Heintz

Department of Mathematical Sciences
Division of Mathematics
Chalmers University of Technology and University of Gothenburg
SE-412 96 Gothenburg, Sweden
Gothenburg, June 2010

Preprint 2010:33
ISSN 1652-9715

Matematiska vetenskaper
Göteborg 2010

Model adaptivity for plates based on a continuous-discontinuous finite element method

David Heintz[1]

[1]*Department of Mathematics*
Chalmers University of Technology and University of Gothenburg
SE-412 96 Göteborg, Sweden

Abstract

A finite element method which combines the Kirchhoff and Mindlin-Reissner plate models is introduced. For this purpose a recently developed family of closely related continuous-discontinuous finite element methods is used: the transverse displacements are approximated by continuous polynomials of degree $d \geq 2$, whereas the rotation vector is approximated by discontinuous polynomials of degree $d-1$. The matrix formulation of the discrete problem is stated. An algorithm is exemplified by simple examples in which the underlying model has been adapted locally in a heuristic manner.

Keywords: Kirchhoff plate; Mindlin-Reissner plate; Nitsche's method; model adaptivity

1 INTRODUCTION

The idea of adapting the underlying physical model for a discrete problem is compelling: the least computationally demanding model in an hierarchy, providing sufficient accuracy, should ideally be used. In the context of plate theory, when considering bending problems for thin to moderately thick structures, the hierarchy would include the Kirchhoff and Mindlin-Reissner (MR) plate models. The former is given by a linear fourth-order partial differential equation (PDE), whose weak formulation typically requires continuous first-order derivatives. However, the conforming approximation can be cumbersome to construct, e.g., a well-known $\mathcal{C}^1$ element, the Argyris triangle, carries 21 degrees of freedom for a quintic approximation. In this paper the focus is different: a continuous-discontinuous Galerkin (c/dG) finite element method (FEM) is used. It was first proposed by Engel *et. al.* [1], and further developed for the Kirchhoff plate theory by Hansbo and Larson [5, 4]. The c/dG FEM is based on a continuous polynomial approximation of degree d for the transverse displacement, but rather than being a property of the approximating space, the continuity in the normal derivatives is enforced weakly by means of Nitsche's method [6]. The MR plate theory, which is an enhanced model by accounting for first-order shear effects, in fact seems simpler from an implementation point-of-view: it consists of a system of two second-order PDEs, and thus only requires a $\mathcal{C}^0$ approximation. Nevertheless, for a FEM to work asymptotically, as the thickness of the plate tends to zero, the approximating spaces for the transverse displacement and the rotation vector need to match. Should their difference not vanish, the numerical solution is degraded by shear locking, caused by an increasing shear energy. Hansbo and Larson [2] proposed a c/dG FEM which avoids shear locking, where the rotation vector is approximated explicitly by discontinuous polynomials of degree $d-1$: in the limit the MR model

simply transposes into the original Kirchhoff model. Consequently, there is the means to construct a low-order c/dG FEM for combing the Kirchhoff and MR plate models; by doing so this paper extends previous work with applications to model adaptivity in mind. The method is advocated as straightforward to implement by the formulation the discrete matrix problem. Lastly, the suggested c/dG FEM is exemplified by simple problems, where the local model is refined by substituting Kirchhoff elements for MR elements.

2 THE CONTINUOUS PROBLEMS

The continuous problems for the Kirchhoff and MR plate models—the strong and the corresponding variational formulations—are introduced under the following assumptions: the domain Ω is a convex polygon, clamped at its boundary $\partial\Omega$, such that $u|_{\partial\Omega}= 0$ and $\boldsymbol{n} \cdot \nabla u|_{\partial\Omega}= 0$; the constitutive parameters and the plate thickness are constants.

The standard plate theory, established by Kirchhoff, is described mathematically by the fourth-order PDE

$$\sum_{ij} \frac{\partial^2 \boldsymbol{\sigma}_{ij}(\nabla u)}{\partial x_i \partial x_j} = f, \quad \text{in } \Omega \subset \mathbb{R}^2, \tag{1}$$

which expresses equilibrium between internal and external forces. u is understood to be the transverse displacement, whereas $\boldsymbol{\sigma}$ represents the moment tensor,

$$\boldsymbol{\sigma}(\nabla u) := \lambda \nabla \cdot \nabla u \mathbf{1} + 2\mu \boldsymbol{\varepsilon}(\nabla u),$$

given the constitutive relation corresponding to a linearly elastic material. Here $\mathbf{1}$ is the identity tensor, and $\boldsymbol{\varepsilon}$ is the curvature tensor, whose components are

$$\boldsymbol{\varepsilon}_{ij} := \frac{1}{2}\left(\frac{\partial^2 u}{\partial x_i \partial x_j} + \frac{\partial^2 u}{\partial x_j \partial x_i} \right), \quad \text{for } i, j = 1, 2.$$

The constitutive parameters are defined by

$$\lambda = \frac{E\nu}{12(1-\nu)^2}, \quad \mu = \frac{E}{24(1+\nu)},$$

where E and ν are Young's modulus and Poisson's ratio, respectively. From (1) $t^3 f$ is recognized as the surface load, acting on a plate with thickness t.

For thicker plates, however, the accuracy of the Kirchhoff solution tends to decay. The model is then commonly replaced by the MR plate theory,

$$\begin{aligned} -\nabla \cdot \boldsymbol{\sigma}(\boldsymbol{\theta}) - \kappa t^{-2}(\nabla u - \boldsymbol{\theta}) &= \mathbf{0}, \\ -\kappa t^{-2} \nabla \cdot (\nabla u - \boldsymbol{\theta}) &= f, \end{aligned} \tag{2}$$

where $\boldsymbol{\theta}$ denotes the rotation of the median surface of the plate, the material parameter $\kappa = Ek/(2(1+v))$, and $k = 5/6$ is a shear correction factor.

The virtual work equation related to (2) can be derived by minimizing the sum of the bending energy, the potential of the surface load, and the shear energy:

$$(u, \boldsymbol{\theta}) = \min_{v, \boldsymbol{\vartheta}} \mathfrak{F}(v, \boldsymbol{\vartheta}) = \tfrac{1}{2} a(\boldsymbol{\vartheta}, \boldsymbol{\vartheta}) + \tfrac{1}{2} b(v, \boldsymbol{\vartheta};\, v, \boldsymbol{\vartheta}) - (f, v)_\Omega. \tag{3}$$

Here v and $\boldsymbol{\vartheta}$ belong to admissible function spaces, and $(\cdot,\cdot)_\Omega$ represents the L_2 inner product over the indicated domain. The bending energy is defined in terms of the tensor contraction

$$a(\boldsymbol{\theta},\boldsymbol{\vartheta}) := \int_\Omega \boldsymbol{\sigma}(\boldsymbol{\theta}) : \boldsymbol{\varepsilon}(\boldsymbol{\vartheta})\,\mathrm{d}\boldsymbol{x}, \tag{4}$$

and the shear energy using

$$b(u,\boldsymbol{\theta};\, v,\boldsymbol{\vartheta}) := \kappa t^{-2}(\nabla u - \boldsymbol{\theta}, \nabla v - \boldsymbol{\vartheta})_\Omega. \tag{5}$$

By omitting $b(\cdot,\cdot;\cdot,\cdot)$ and substituting $\boldsymbol{\vartheta} = \nabla v$ in (3), the corresponding minimization problem for the Kirchhoff plate theory is obtained. Notice that when the displacement gradient equals the rotation vector, higher regularity is required of the solution, owing to the second-order derivatives present in the bilinear form (4). Solving (3) yields the equivalent variational formulations: find $u_K \in V(\Omega)$ and $(u_M,\boldsymbol{\theta}) \in H_0^1(\Omega)\times[H_0^1(\Omega)]^2$ such that

$$\begin{aligned} a(\nabla u_K, \nabla v) &= (f,v)_\Omega, \quad \text{for all } v \in V(\Omega),\\ a(\boldsymbol{\theta},\boldsymbol{\vartheta}) + b(u_M,\boldsymbol{\theta};v,\boldsymbol{\vartheta}) &= (f,v)_\Omega, \quad \text{for all } (v,\boldsymbol{\vartheta}) \in H_0^1(\Omega)\times[H_0^1(\Omega)]^2, \end{aligned}$$

where the function space $V = \{v \in H_0^2(\Omega) : \boldsymbol{n}\cdot\nabla v = 0 \text{ on } \partial\Omega\}$.

3 THE DISCRETE PROBLEMS

3.1 The mesh

Consider the partition $\mathfrak{T}_h = \{T\}$ of Ω into a geometrically conforming, quasi-uniform finite element triangulation. Let h_T denote the local mesh size

$$h_T = \operatorname{diam}(T) = \max_{\boldsymbol{y}_1,\boldsymbol{y}_2\in T} \|\boldsymbol{y}_1 - \boldsymbol{y}_2\|, \quad \text{for all } T \in \mathfrak{T}_h,$$

and have

$$h = \max_{T\in\mathfrak{T}_h} h_T$$

to be the global mesh size parameter. Moreover, define a set $\mathfrak{E} = \{E\}$ to represent the edges in the mesh, which can be divided into two disjoint subsets, $\mathfrak{E} = \mathfrak{E}_I \cup \mathfrak{E}_B$, where $\mathfrak{E}_I = \mathfrak{E} \setminus \partial\Omega$ and $\mathfrak{E}_B$ are the sets of interior and boundary edges, respectively. Each edge is associated with a fixed unit normal $\boldsymbol{n}$, such that on the boundary, $\boldsymbol{n}$ is the exterior unit normal.

3.2 Function spaces

The function space

$$V_h := \left\{v \in H_0^1(\Omega) :\, v|_T \in \mathcal{P}_d(T) \text{ for all } T \in \mathfrak{T}_h\right\}$$

of continuous, piecewise polynomials of degree d, that vanish on the boundary, is used to approximate the transverse displacement. Likewise, for the rotation vector,

$$\boldsymbol{\Theta}_h := \left\{\boldsymbol{\vartheta} \in [L_2(\Omega)]^2 :\, \boldsymbol{\vartheta}|_T \in [\mathcal{P}_{d-1}(T)]^2 \text{ for all } T \in \mathfrak{T}_h\right\}$$

is the function space of discontinuous polynomials of degree $d-1$. The choice of approximating spaces, as mentioned by Hansbo *et. al.* [3, Section 3], makes them compatible in the sense that

$$\nabla v \subset \boldsymbol{\Theta}_h, \quad \text{for all } v \in V_h.$$

This property is important, since in the limit as $t \to 0$, it allows for functions in $\boldsymbol{\Theta}_h$ to belong to ∇V_h. Hence there exists non-trivial approximations, such that the difference $\nabla u - \boldsymbol{\theta}$ in the shear energy functional (5) vanishes, and consequently shear locking is alleviated. Another idea would be to replace the rotation vector in (5) by a suitable projection. This approach was introduced by Bathe *et. al.* [8]; the associated MITC element family has been further described in the literature [9, Section 5.4].

3.3 Jumps and averages

Two quantities on $\mathfrak{E}$ are introduced: the jump $[\![\cdot]\!]$ and the average $\langle\cdot\rangle$. To this end, let T_1 and T_2 be two neighboring elements, sharing the interior edge E. For a scalar function $v \in V_h$ define

$$
\begin{aligned}
[\![v]\!] &:= v^- - v^+, \quad \text{for } E \in \mathfrak{E}_I, & [\![v]\!] &:= v^-, \quad \text{for } E \in \mathfrak{E}_B, \\
\langle v \rangle &:= \frac{v^- + v^+}{2}, \quad \text{for } E \in \mathfrak{E}_I, & \langle v \rangle &:= v^-, \quad \text{for } E \in \mathfrak{E}_B,
\end{aligned}
$$

where

$$
v^- = \lim_{\epsilon \to 0^+} v(\boldsymbol{x} - \epsilon \boldsymbol{n}), \quad v^+ = \lim_{\epsilon \to 0^+} v(\boldsymbol{x} + \epsilon \boldsymbol{n}), \quad \text{for } \boldsymbol{x} \in E.
$$

The definitions for a vector-valued function $\boldsymbol{\vartheta} \in \boldsymbol{\Theta}_h$ are analogous.

3.4 The finite element method

The c/dG FEMs can now be formulated as follows: find $u_K^h \in V_h$ and $(u_M^h, \boldsymbol{\theta}^h) \in V_h \times \boldsymbol{\Theta}_h$ such that

$$
a_h(\nabla u_K^h, \nabla v) = (f, v)_\Omega, \quad \text{for all } v \in V_h, \tag{6}
$$

$$
a_h(\boldsymbol{\theta}^h, \boldsymbol{\vartheta}) + b(u_M^h, \boldsymbol{\theta}^h;\, v, \boldsymbol{\vartheta}) = (f, v)_\Omega, \quad \text{for all } (v, \boldsymbol{\vartheta}) \in V_h \times \boldsymbol{\Theta}_h, \tag{7}
$$

where the discrete bilinear form—which stems from using Nitsche's method (see e.g. [5])—is defined by

$$
\begin{aligned}
a_h(\boldsymbol{\theta}^h, \boldsymbol{\vartheta}) := \sum_{T \in \mathfrak{T}_h} \int_T \boldsymbol{\sigma}(\boldsymbol{\theta}^h) : \boldsymbol{\varepsilon}(\boldsymbol{\vartheta}) \, \mathrm{d}\boldsymbol{x} - \sum_{E \in \mathfrak{E}} (\langle \boldsymbol{n} \cdot \boldsymbol{\sigma}(\boldsymbol{\theta}^h) \rangle, [\![\boldsymbol{\vartheta}]\!])_E \\
- \sum_{E \in \mathfrak{E}} (\langle \boldsymbol{n} \cdot \boldsymbol{\sigma}(\boldsymbol{\vartheta}) \rangle, [\![\boldsymbol{\theta}^h]\!])_E + (2\mu + 2\lambda)\gamma \sum_{E \in \mathfrak{E}} (h_E^{-1} [\![\boldsymbol{\theta}^h]\!], [\![\boldsymbol{\vartheta}]\!])_E.
\end{aligned} \tag{8}
$$

The last term in (8) penalizes jumps in the rotation vector, or the displacement gradient, across element edges. Its stabilization parameter γ must be chosen large enough to enforce coercivity on $a_h(\cdot, \cdot)$; the *penalty term* in this sense controls the other edge integrals, the first of whom makes the formulation consistent, whereas the addition of the second brings symmetry[1]. (They will be referred to collectively as the *symmetry terms*.) Precise values of γ, for an arbitrary polynomial approximation $d \geq 2$, have been calculated by Hansbo and Larson [4, Section 2.3] for the Kirchhoff plate model. Further analysis [3, Section 4] shows that the results are valid also for the MR plate model (the presence of the shear energy functional (5) in (7) rather stabilizes the numerical problem by being an inner product.) Lastly, h_E is given by

$$
h_E = \begin{cases} \frac{|T_1| + |T_2|}{2|E|}, & \text{for } E \in \mathfrak{E}_I, \\ |T|/|E|, & \text{for } E \in \mathfrak{E}_B, \end{cases}
$$

[1] If applying a direct method to the discrete linear system, the stiffness matrix can now be subjected to Cholesky factorization.

where $|\cdot|$ denotes the area of T or the length of E.

4 IMPLEMENTATION

To define the method when combing both plate models, i.e., how to combine (6) and (7), the resulting matrix problem $\mathbf{S}\omega = \mathbf{f}$ is considered. For simplicity the lowest-order scheme is applied with $d = 2$, and the basis consists of standard Lagrange finite element shape functions. Hence all elements $T \in \mathfrak{T}_h$ carries six degrees of freedom associated with the transverse displacements, and should T be an MR element, another six related to the rotation vector. The local element and edge matrices, which are assembled into the global stiffness matrix $\mathbf{S}$, are constructed. Note then that the suggested c/dG FEM employs the same trial and test spaces. Finally a simple refinement criterion is introduced to exemplify the use of the method in a model adaptive context.

4.1 Kirchhoff plate model

4.1.1 Domain integral

Consider the domain integral of the bilinear form (8). The integrand can be rewritten using the Voigt form in the symmetric tensor contraction,

$$\int_T \boldsymbol{\sigma}(\nabla u_K^h) : \boldsymbol{\varepsilon}(\nabla v)\,\mathrm{d}\boldsymbol{x} = \int_T \boldsymbol{\varepsilon}_{\mathrm{v}}^{\mathrm{T}}(\nabla u_K^h)\boldsymbol{D}\boldsymbol{\varepsilon}(\nabla v)\,\mathrm{d}\boldsymbol{x}, \tag{9}$$

where

$$\boldsymbol{\varepsilon}_{\mathrm{v}}(\nabla u_K^h) = \begin{bmatrix} \frac{\partial^2 u_K^h}{\partial x_1^2} \\ \frac{\partial^2 u_K^h}{\partial x_2^2} \\ 2\frac{\partial^2 u_K^h}{\partial x_1 \partial x_2} \end{bmatrix} = \begin{bmatrix} \frac{\partial^2 \varphi_1}{\partial x_1^2} & \cdots & \frac{\partial^2 \varphi_6}{\partial x_1^2} \\ \frac{\partial^2 \varphi_1}{\partial x_2^2} & \cdots & \frac{\partial^2 \varphi_6}{\partial x_2^2} \\ 2\frac{\partial^2 \varphi_1}{\partial x_1 \partial x_2} & \cdots & 2\frac{\partial^2 \varphi_6}{\partial x_1 \partial x_2} \end{bmatrix} \begin{bmatrix} u_1 \\ \vdots \\ u_6 \end{bmatrix} = \hat{\boldsymbol{B}}_T \mathbf{u}_T.$$

Here $\{\varphi_i\} \in V_h$ are the local shape functions on element T, whereas $\mathbf{u}_T$ represents its nodal transverse displacements, and the constitutive matrix is defined by

$$\boldsymbol{D} = \begin{bmatrix} \lambda + 2\mu & \lambda & 0 \\ \lambda & \lambda + 2\mu & 0 \\ 0 & 0 & \mu \end{bmatrix}.$$

Next substitute $\nabla v = \nabla \varphi_i$ in (9) for $i = 1, \ldots, 6$, on which the integrand becomes constant, and the element contribution to the stiffness matrix reduces to

$$\hat{\mathbf{S}}_T = |T| \hat{\boldsymbol{B}}_T^{\mathrm{T}} \boldsymbol{D} \hat{\boldsymbol{B}}_T, \quad \text{for all } T \in \mathfrak{T}_h. \tag{10}$$

4.1.2 Symmetry terms

Firstly, at an interior edge common to the neighbors T_1 and T_2, consider

$$\boldsymbol{n} \cdot \boldsymbol{\sigma}(\nabla u_K^h) = \begin{bmatrix} n_1\sigma_{11} + n_2\sigma_{12} \\ n_1\sigma_{21} + n_2\sigma_{22} \end{bmatrix} = \begin{bmatrix} n_1 & 0 & n_2 \\ 0 & n_2 & n_1 \end{bmatrix} \boldsymbol{D}\hat{\boldsymbol{B}}_T \mathbf{u}_T = \boldsymbol{N}\boldsymbol{D}\hat{\boldsymbol{B}}_T \mathbf{u}_T,$$

where $\boldsymbol{n} = [n_1,\ n_2]^{\mathrm{T}}$ is the exterior unit normal to T_1 on E. Let $\hat{\boldsymbol{B}}_{T_i}$ and $\mathbf{u}_{T_i}$ be defined on the i:th element. Now the average is

$$\langle \boldsymbol{n} \cdot \boldsymbol{\sigma}(\nabla u_K^h) \rangle = \tfrac{1}{2}\boldsymbol{N}\boldsymbol{D}(\hat{\boldsymbol{B}}_{T_1}\mathbf{u}_{T_1} + \hat{\boldsymbol{B}}_{T_2}\mathbf{u}_{T_2}) = \tfrac{1}{2}\boldsymbol{N}\boldsymbol{D}\hat{\boldsymbol{B}}_{\mathrm{tot}}\mathbf{u}_{\mathrm{tot}}, \tag{11}$$

with $\hat{\boldsymbol{B}}_{\text{tot}} = [\hat{\boldsymbol{B}}_{T_1},\ \hat{\boldsymbol{B}}_{T_2}]$ and $\mathbf{u}_{\text{tot}} = [\mathbf{u}_{T_1}^{\mathrm{T}},\ \mathbf{u}_{T_2}^{\mathrm{T}}]^{\mathrm{T}}$. At a boundary edge the average (11) simplifies to $\langle \boldsymbol{n} \cdot \boldsymbol{\sigma}(\nabla u_K^h) \rangle = \boldsymbol{N}\boldsymbol{D}\hat{\boldsymbol{B}}_T \mathbf{u}_T$. The introduction of the gradient matrix

$$\boldsymbol{G}_T = \begin{bmatrix} \frac{\partial \varphi_1}{\partial x_1} & \cdots & \frac{\partial \varphi_6}{\partial x_1} \\ \frac{\partial \varphi_1}{\partial x_2} & \cdots & \frac{\partial \varphi_6}{\partial x_2} \end{bmatrix},$$

allows writing $\nabla u_K^h = \boldsymbol{G}_T \mathbf{u}_T$. Consequently, at an interior edge, the related jump is

$$[\![\nabla u_K^h]\!] = \boldsymbol{G}_{T_1} \mathbf{u}_{T_1} - \boldsymbol{G}_{T_2} \mathbf{u}_{T_2} = \boldsymbol{G}_{\text{tot}} \mathbf{u}_{\text{tot}}, \tag{12}$$

where $\boldsymbol{G}_{\text{diff}} = [\boldsymbol{G}_{T_1},\ -\boldsymbol{G}_{T_2}]$. Similarly, at a boundary edge, (12) reduces to $[\![\nabla u_K^h]\!] = \boldsymbol{G}_T \mathbf{u}_T$. Hence the integrands of the symmetry terms in (8) follow as

$$\langle \boldsymbol{n} \cdot \boldsymbol{\sigma}(\nabla u_K^h) \rangle \cdot [\![\nabla v]\!] = \begin{cases} \frac{1}{2} \boldsymbol{G}_{\text{diff}}^{\mathrm{T}} \boldsymbol{N}\boldsymbol{D}\hat{\boldsymbol{B}}_{\text{tot}} \mathbf{u}_{\text{tot}}, & \text{for } E \in \mathfrak{E}_I, \\ \boldsymbol{G}_T^{\mathrm{T}} \boldsymbol{N}\boldsymbol{D}\hat{\boldsymbol{B}}_T \mathbf{u}_T, & \text{for } E \in \mathfrak{E}_B, \end{cases}$$

when testing against the local shape functions: either the union of $\{\varphi_i\}$ on T_1 and $\{\varphi_j\}$ on T_2 for $E \in \mathfrak{E}_I$, or $\{\varphi_i\}$ on T for $E \in \mathfrak{E}_B$. In the sequel a shorter notation is adopted,

$$\langle \boldsymbol{n} \cdot \boldsymbol{\sigma}(\nabla u_K^h) \rangle \cdot [\![\nabla v]\!] = \alpha_\star \hat{\boldsymbol{\Sigma}}_\star \mathbf{u}_\star,$$

in this case by letting $\hat{\boldsymbol{\Sigma}}_\star = \boldsymbol{G}_\star^{\mathrm{T}} \boldsymbol{N}\boldsymbol{D}\hat{\boldsymbol{B}}_\star$. When a quantity is indexed accordingly ($\star$) it can be evaluated at any edge $E \in \mathfrak{E}$; thus

$$\langle \boldsymbol{n} \cdot \boldsymbol{\sigma}(\nabla v) \rangle \cdot [\![\nabla u_K^h]\!] = \begin{cases} \alpha_I \hat{\boldsymbol{\Sigma}}_{\text{tot}}^{\mathrm{T}} \mathbf{u}_{\text{tot}}, & \text{for } E \in \mathfrak{E}_I, \\ \alpha_B \hat{\boldsymbol{\Sigma}}_T^{\mathrm{T}} \mathbf{u}_T, & \text{for } E \in \mathfrak{E}_B, \end{cases}$$

with $\alpha_I = 1/2$ and $\alpha_B = 1$. Thereby the edge contributions to the stiffness matrix, $\hat{\mathbf{S}}_I^{\text{sym}}$ and $\hat{\mathbf{S}}_B^{\text{sym}}$, can be written

$$\hat{\mathbf{S}}_\star^{\text{sym}} = \int_E \alpha_\star \left(\hat{\boldsymbol{\Sigma}}_\star + \hat{\boldsymbol{\Sigma}}_\star^{\mathrm{T}} \right) \mathrm{d}\boldsymbol{s}, \quad \text{for all } E \in \mathfrak{E}, \tag{13}$$

for short.

4.1.3 Penalty term

From (12) it is clear that

$$[\![\nabla u_K^h]\!] \cdot [\![\nabla v]\!] = \begin{cases} \boldsymbol{G}_{\text{diff}}^{\mathrm{T}} \boldsymbol{G}_{\text{diff}} \mathbf{u}_{\text{tot}}, & \text{for } E \in \mathfrak{E}_I, \\ \boldsymbol{G}_T^{\mathrm{T}} \boldsymbol{G}_T \mathbf{u}_T, & \text{for } E \in \mathfrak{E}_B, \end{cases}$$

when testing against the local shape functions, and the edge contributions to the stiffness matrix, $\hat{\mathbf{S}}_I^{\text{p}}$ and $\hat{\mathbf{S}}_B^{\text{p}}$, are readily identified by

$$\hat{\mathbf{S}}_\star^{\text{p}} = (2\mu + 2\lambda)\gamma \int_E h_E^{-1} \boldsymbol{G}_\star^{\mathrm{T}} \boldsymbol{G}_\star \, \mathrm{d}\boldsymbol{s}, \quad \text{for all } E \in \mathfrak{E}. \tag{14}$$

4.2 Mindlin-Reissner plate model

4.2.1 Domain integrals

The integrand emanating from $a_h(\cdot,\cdot)$ has the same form as (9), with the displacement gradient being replaced by the discrete rotation vector $\boldsymbol{\theta}^h = [\theta^x,\ \theta^y]^{\mathrm{T}}$ (here $x = x_1$ and $y = x_2$ are used as indices to distinguish coordinate axes from local node numbers). Hence consider

$$\begin{aligned}\boldsymbol{\varepsilon}_{\mathrm{v}}(\boldsymbol{\theta}^h) &= \begin{bmatrix} \frac{\partial\theta^x}{\partial x_1} \\ \frac{\partial\theta^y}{\partial x_2} \\ \frac{\partial\theta^x}{\partial x_2} + \frac{\partial\theta^y}{\partial x_1} \end{bmatrix} = \begin{bmatrix} \frac{\partial\vartheta_1}{\partial x_1} & 0 & \frac{\partial\vartheta_2}{\partial x_1} & 0 & \frac{\partial\vartheta_3}{\partial x_1} & 0 \\ 0 & \frac{\partial\vartheta_1}{\partial x_2} & 0 & \frac{\partial\vartheta_2}{\partial x_2} & 0 & \frac{\partial\vartheta_3}{\partial x_2} \\ \frac{\partial\vartheta_1}{\partial x_2} & \frac{\partial\vartheta_1}{\partial x_1} & \frac{\partial\vartheta_2}{\partial x_2} & \frac{\partial\vartheta_2}{\partial x_1} & \frac{\partial\vartheta_3}{\partial x_2} & \frac{\partial\vartheta_3}{\partial x_1} \end{bmatrix} \begin{bmatrix} \theta_1^x & \theta_1^y & \theta_2^x & \theta_2^y & \theta_3^x & \theta_3^y \end{bmatrix}^{\mathrm{T}} \\ &= \tilde{\boldsymbol{B}}_T \theta_T,\end{aligned}$$

where $\{\vartheta_i\}$ are the *linear* Lagrange finite element shape functions[2]. θ_T represents the nodal rotation components on element T. Consequently,

$$\int_T \boldsymbol{\sigma}(\boldsymbol{\theta}^h) : \boldsymbol{\varepsilon}(\boldsymbol{\vartheta})\,\mathrm{d}\boldsymbol{x} = \int_T \boldsymbol{\varepsilon}_{\mathrm{v}}^{\mathrm{T}}(\boldsymbol{\theta}^h)\boldsymbol{D}\boldsymbol{\varepsilon}(\boldsymbol{\vartheta})\,\mathrm{d}\boldsymbol{x} = |T|\tilde{\boldsymbol{B}}_T^{\mathrm{T}}\boldsymbol{D}\tilde{\boldsymbol{B}}_T\theta_T,$$

following substitution of $\boldsymbol{\vartheta}$ for the local shape functions, i.e., each column vector in

$$\boldsymbol{R} = \begin{bmatrix} \vartheta_1 & 0 & \vartheta_2 & 0 & \vartheta_3 & 0 \\ 0 & \vartheta_1 & 0 & \vartheta_2 & 0 & \vartheta_3 \end{bmatrix}. \tag{15}$$

Furthermore, from the shear energy functional (5),

$$(\nabla u_M^h - \boldsymbol{\theta}^h, \nabla v - \boldsymbol{\vartheta})_\Omega = (\nabla v, \nabla u_M^h)_\Omega - (\boldsymbol{\vartheta}, \nabla u_M^h)_\Omega - (\nabla v, \boldsymbol{\theta}^h)_\Omega + (\boldsymbol{\vartheta}, \boldsymbol{\theta}^h)_\Omega, \tag{16}$$

and by introducing the matrices

$$\boldsymbol{V} = \begin{bmatrix} \boldsymbol{G} & -\boldsymbol{R} \end{bmatrix}, \quad \omega_T = \begin{bmatrix} \mathbf{u}_T & \theta_T \end{bmatrix}^{\mathrm{T}},$$

the expansion (16), by substituting the test functions appropriately, can be rewritten as

$$(\boldsymbol{G}^{\mathrm{T}}\boldsymbol{G} - \boldsymbol{R}^{\mathrm{T}}\boldsymbol{G})\mathbf{u}_T + (\boldsymbol{R}^{\mathrm{T}}\boldsymbol{R} - \boldsymbol{G}^{\mathrm{T}}\boldsymbol{R})\theta_T = \boldsymbol{V}^{\mathrm{T}}\boldsymbol{V}\omega_T.$$

Hence it is that

$$\kappa t^{-2}(\nabla u_M^h - \boldsymbol{\theta}^h, \nabla v - \boldsymbol{\vartheta})_\Omega = \kappa t^{-2}\int_T \boldsymbol{V}^{\mathrm{T}}\boldsymbol{V}\,\mathrm{d}\boldsymbol{x}\,\omega_T,$$

and the element contribution to the stiffness matrix becomes

$$\tilde{\mathbf{S}}_T = \tilde{\mathbf{S}}_T^a + \tilde{\mathbf{S}}_T^b = |T|\tilde{\boldsymbol{B}}^{\mathrm{T}}\boldsymbol{D}\tilde{\boldsymbol{B}} + \kappa t^{-2}\int_T \boldsymbol{V}^{\mathrm{T}}\boldsymbol{V}\,\mathrm{d}\boldsymbol{x}, \quad \text{for all } T \in \mathfrak{T}_h, \tag{17}$$

where $\tilde{\mathbf{S}}_T^b$, as opposed to the constant $\tilde{\mathbf{S}}_T^a$, is computed using numerical quadrature.

[2] A simple alternative would be to use the set of monomials for local shape functions, so long as no direct physical interpretation is of convenience, say for purposes of visualization and/or interpolation.

4.2.2 Symmetry terms

In the same manner as for the Kirchhoff plate model the averages are derived to be

$$\langle \boldsymbol{n} \cdot \boldsymbol{\sigma}(\boldsymbol{\theta}^h) \rangle = \begin{cases} \frac{1}{2} \boldsymbol{N}\boldsymbol{D}\tilde{\boldsymbol{B}}_{\text{tot}}\theta_{\text{tot}}, & \text{for } E \in \mathfrak{E}_I, \\ \boldsymbol{N}\boldsymbol{D}\tilde{\boldsymbol{B}}_T\theta_T, & \text{for } E \in \mathfrak{E}_B, \end{cases} \tag{18}$$

where $\tilde{\boldsymbol{B}}_{\text{tot}} = [\tilde{\boldsymbol{B}}_{T_1},\ \tilde{\boldsymbol{B}}_{T_2}]$ and $\theta_{\text{tot}} = [\theta_{T_1}^{\mathrm{T}},\ \theta_{T_2}^{\mathrm{T}}]^{\mathrm{T}}$. The corresponding jumps in the rotation components are

$$[\![\boldsymbol{\theta}^h]\!] = \begin{cases} \boldsymbol{R}_{\text{diff}}\theta_{\text{tot}}, & \text{for } E \in \mathfrak{E}_I, \\ \boldsymbol{R}_T\theta_T, & \text{for } E \in \mathfrak{E}_B, \end{cases} \tag{19}$$

for $\boldsymbol{R}_{\text{diff}} = [\boldsymbol{R}_{T_1}\ -\boldsymbol{R}_{T_2}]$ with $\boldsymbol{R}_{T_i}$ defined as in (15) on element T_i. Now if combing (18) and (19), with $\tilde{\boldsymbol{\Sigma}}_\star = \boldsymbol{R}_\star^{\mathrm{T}}\boldsymbol{N}\boldsymbol{D}\tilde{\boldsymbol{B}}_\star$, it follows that

$$\langle \boldsymbol{n} \cdot \boldsymbol{\sigma}(\boldsymbol{\theta}^h) \rangle \cdot [\![\boldsymbol{\vartheta}]\!] = \alpha_\star \tilde{\boldsymbol{\Sigma}}_\star \theta_\star, \quad \langle \boldsymbol{n} \cdot \boldsymbol{\sigma}(\boldsymbol{\vartheta}) \rangle \cdot [\![\boldsymbol{\theta}^h]\!] = \alpha_\star \tilde{\boldsymbol{\Sigma}}_\star^{\mathrm{T}} \theta_\star,$$

when testing against the local shape functions. The edge contributions to the stiffness matrix, $\tilde{\mathbf{S}}_I^{\text{sym}}$ and $\tilde{\mathbf{S}}_B^{\text{sym}}$, become

$$\tilde{\mathbf{S}}_\star^{\text{sym}} = \int_E \alpha_\star \left(\tilde{\boldsymbol{\Sigma}}_\star + \tilde{\boldsymbol{\Sigma}}_\star^{\mathrm{T}} \right) \mathrm{d}\boldsymbol{s}, \quad \text{for all } E \in \mathfrak{E}. \tag{20}$$

4.2.3 Penalty term

Using (19) the product between the jumps

$$[\![\boldsymbol{\theta}^h]\!] \cdot [\![\boldsymbol{\vartheta}]\!] = \begin{cases} \boldsymbol{R}_{\text{diff}}^{\mathrm{T}}\boldsymbol{R}_{\text{diff}}\theta_{\text{tot}}, & \text{for } E \in \mathfrak{E}_I, \\ \boldsymbol{R}_T^{\mathrm{T}}\boldsymbol{R}_T\theta_T, & \text{for } E \in \mathfrak{E}_B, \end{cases}$$

when testing against the local basis functions, and so the edge contributions to the stiffness matrix, $\tilde{\mathbf{S}}_I^{\text{p}}$ and $\tilde{\mathbf{S}}_B^{\text{p}}$, are

$$\tilde{\mathbf{S}}_\star^{\text{p}} = (2\mu + 2\lambda)\gamma \int_E h_E^{-1} \boldsymbol{R}_\star^{\mathrm{T}} \boldsymbol{R}_\star \, \mathrm{d}\boldsymbol{s}, \quad \text{for all } E \in \mathfrak{E}. \tag{21}$$

4.3 Combined plate models

Note that the plate models are combined only on interior edges—the domain and boundary integrals of the bilinear form are evaluated using either the Kirchhoff or the MR plate model. Let $\boldsymbol{\theta}^h$ and $\boldsymbol{\vartheta}$ denote the discrete solution vector and the combined basis functions (even though half of the associated degrees of freedom relate to displacements).

4.3.1 Symmetry terms

It is important to keep in mind which plate model is used locally: the average will be

$$\langle \boldsymbol{n} \cdot \boldsymbol{\sigma}(\boldsymbol{\theta}^h) \rangle = \begin{cases} \frac{1}{2} \boldsymbol{N}\boldsymbol{D}\boldsymbol{B}_1\omega_1, & \text{if } T_1 \text{ is a Kirchhoff element}, \\ \frac{1}{2} \boldsymbol{N}\boldsymbol{D}\boldsymbol{B}_2\omega_2, & \text{if } T_1 \text{ is a MR element}, \end{cases} \tag{22}$$

where $\boldsymbol{B}_1 = [\hat{\boldsymbol{B}}_{T_1},\ \tilde{\boldsymbol{B}}_{T_2}]$, $\boldsymbol{B}_2 = [\tilde{\boldsymbol{B}}_{T_1},\ \hat{\boldsymbol{B}}_{T_2}]$, $\omega_1 = [\mathbf{u}_{T_1}^{\mathrm{T}},\ \theta_{T_2}^{\mathrm{T}}]^{\mathrm{T}}$, and $\omega_2 = [\theta_{T_1}^{\mathrm{T}},\ \mathbf{u}_{T_2}^{\mathrm{T}}]^{\mathrm{T}}$. The jump is given by

$$[\![\boldsymbol{\theta}^h]\!] = \begin{cases} \boldsymbol{J}_1\omega_1, & \text{if } T_1 \text{ is a Kirchhoff element,} \\ \boldsymbol{J}_2\omega_2, & \text{if } T_1 \text{ is a MR element,} \end{cases} \tag{23}$$

for $\boldsymbol{J}_1 = [\boldsymbol{G}_{T_1},\ -\boldsymbol{R}_{T_2}]$ and $\boldsymbol{J}_2 = [\boldsymbol{R}_{T_1},\ -\boldsymbol{G}_{T_2}]$. Let $\boldsymbol{\Sigma}_\star = \frac{1}{2}\boldsymbol{J}_\star^{\mathrm{T}}\boldsymbol{N}\boldsymbol{D}\boldsymbol{B}_\star$ and combine (22) and (23) to get

$$\langle \boldsymbol{n}\cdot\boldsymbol{\sigma}(\boldsymbol{\theta}^h)\rangle \cdot [\![\vartheta]\!] = \boldsymbol{\Sigma}_\star\omega_\star, \quad \langle \boldsymbol{n}\cdot\boldsymbol{\sigma}(\vartheta)\rangle \cdot [\![\boldsymbol{\theta}^h]\!] = \boldsymbol{\Sigma}_\star^{\mathrm{T}}\omega_\star,$$

when testing against the (combined) local basis functions. Thus the interior edge contributions to the stiffness matrix, $\mathbf{S}_1^{\mathrm{sym}}$ and $\mathbf{S}_2^{\mathrm{sym}}$, will be

$$\mathbf{S}_\star^{\mathrm{sym}} = \int_E \left(\boldsymbol{\Sigma}_\star + \boldsymbol{\Sigma}_\star^{\mathrm{T}}\right)\,\mathrm{d}\boldsymbol{s}, \quad \text{for all } E \in \mathfrak{E}_I. \tag{24}$$

4.3.2 Penalty term

Following (19) it is that

$$[\![\boldsymbol{\theta}^h]\!] \cdot [\![\vartheta]\!] = \begin{cases} \boldsymbol{J}_1^{\mathrm{T}}\boldsymbol{J}_1\omega_1, & \text{if } T_1 \text{ is a Kirchhoff element,} \\ \boldsymbol{J}_2^{\mathrm{T}}\boldsymbol{J}_2\omega_2, & \text{if } T_1 \text{ is a MR element,} \end{cases}$$

when testing against the (combined) local basis functions, and the edge contributions to the stiffness matrix, $\mathbf{S}_1^{\mathrm{p}}$ and $\mathbf{S}_2^{\mathrm{p}}$, are

$$\mathbf{S}_\star^{\mathrm{p}} = (2\mu + 2\lambda)\gamma \int_E h_E^{-1}\boldsymbol{J}_\star^{\mathrm{T}}\boldsymbol{J}_\star\,\mathrm{d}\boldsymbol{s}, \quad \text{for all } E \in \mathfrak{E}_I. \tag{25}$$

4.4 Load vector

The right-hand side load of the matrix problem is obtained as

$$\mathbf{f} = \sum_T (f, v)_T,$$

and the element contribution is

$$\mathbf{f}_T = (f, v)_T = |T| \sum_i w_i f(\boldsymbol{x}_i)\varphi(\boldsymbol{x}_i), \quad \text{for all } T \in \mathfrak{T}_h, \tag{26}$$

where $\{w_i\}$ and $\{\boldsymbol{x}_i\}$ are the corresponding sets of quadrature weights and abscissas, respectively, and $\varphi = [\varphi_1,\ \ldots, \varphi_6]^{\mathrm{T}}$ is the local basis function vector.

4.5 Model refinement

Now assume that an initial solution u_K^h has been computed. To improve its accuracy MR elements are introduced locally where the transversal force at the edges,

$$T_s = \left(\nabla\cdot\boldsymbol{\sigma}(u_K^h)\right)\cdot\boldsymbol{n} + \partial_t\boldsymbol{M}_{nt}, \tag{27}$$

where ∂_t denotes the tangential derivative operator and $\boldsymbol{M}_{nt} = \boldsymbol{t}\cdot\left(\boldsymbol{\sigma}(u_K^h)\cdot\boldsymbol{n}\right)$ is the twisting moment, is large in magnitude. However, in this case M_{nt} is edgewise constant (when using the lowest-order

scheme with $d = 2$), and in order to approximate its tangential derivative patches of elements must be considered. Thus, for simplicity, take

$$\eta_E := \|[\![\boldsymbol{\sigma}(u_K^h) \cdot \boldsymbol{n}]\!]\|_2 / h, \quad \text{for all } E \in \mathfrak{E}, \tag{28}$$

to substitute (27) as the edge *refinement* indicator. The normal derivative is approximated by the jump in the bending moment divided by either: 1) the centroid-to-centroid distance between the neighbors T_1 and T_2 when $E \in \mathfrak{E}_I$; or 2) the centroid-to-boundary distance on T should $E \in \mathfrak{E}_B$.

A fixed-ratio $0 \leq r \leq 1$ of the Kirchhoff elements carrying the largest refinement indicators η_T will be replaced by MR elements. η_T is obtained by the weighted sum

$$\eta_T = \sum_{i=1}^{3} \alpha_i \eta_{E,i}, \quad \text{with } \eta_{E,i} \text{ as in (28) for } E \subset \partial T, \tag{29}$$

where $\alpha_i = 1/2$ if $E \in \mathfrak{E}_I$ (the edge refinement indicator is split equally between neighbors) and $\alpha_i = 1$ otherwise. The accuracy of the improved displacement approximation u_C^h is compared to that of u_K^h in terms of the global L_2 norm of the relative error,

$$e = \left(u - u_\star^h, u - u_\star^h\right)_\Omega^{1/2} / (u, u)_\Omega^{1/2},$$

with u as the exact solution of (2).

It is stressed that (28) is nothing but a heuristic measure; an actual *error* indicator should be based on duality techniques, in which both discretization and modeling errors are estimated, with respect to a user-specified goal quantity (a functional of the numerical solution). (28) provides no error control, and its sole purpose is to hint where the numerical solution may benefit from local model refinement.

4.6 Adaptive algorithm

A way to organize the computations is presented in Algorithm 1. The implementation may be aided by the following practical advices:

- Let the solution vector store degrees of freedom associated with transverse displacements first, and then for each introduced MR element, add its rotational degrees of freedom in consecutive order (no renumbering of the degrees of freedom is required).
- The computational cost for solving the additional matrix problem, when combing plate models, can be reduced by using a sparse storage format during the assembly processes. If relying on a COO format, i.e., storing non-zero elements $\mathbf{S}_{ij}$ in a list of (`row`, `column`, `value`) tuples, only entries associated with refined elements and edges need to be reassembled. For h-adaptivity this is possible albeit less straightforward. Note also that the load vector $\mathbf{f}$ need not be recomputed; it can simply be padded with as many zeros as the number of added rotational degrees of freedom. The largest cost, however, ought to come from solving the larger linear system and not from its construction.

5 NUMERICAL EXAMPLES

Consider an isotropic and homogeneous material, represented by the unit square $\Omega = [0,\, 1] \times [0,\, 1]$. The plate is clamped at the boundary $\partial\Omega = \{(x_1, x_2) : x_1 = 0,\ x_1 = 1,\ x_2 = 0,\ x_2 = 1\}$, and is

Algorithm 1: Model adaptive scheme

Data: triangulation $\{T\} = \mathfrak{T}_h$ and associated edges $\{E\} = \mathfrak{E}$
Result: FE solutions u_K^h and $\omega = (u_C^h,\ \boldsymbol{\theta}_C^h)$

Kirchhoff plate model
forall $T \in \mathfrak{T}_h$ **do**
  assemble element stiffness matrix $\hat{\mathbf{S}}_T$ according to (10)
  assemble element load vector $\mathbf{f}_T$ using (26)
end
forall $E \in \mathfrak{E}$ **do**
  assemble symmetry edge matrices $\hat{\mathbf{S}}_I^{\text{sym}}$ and $\hat{\mathbf{S}}_B^{\text{sym}}$via (13)
  assemble penalty edge matrices $\hat{\mathbf{S}}_I^{\text{p}}$ and $\hat{\mathbf{S}}_B^{\text{p}}$ according to (14)
end
construct sparse stiffness matrix $\mathbf{S}_K$
solve linear system $\mathbf{u}_K^h = \mathbf{S}_K^{-1}\mathbf{f}_K$ (use that $\mathbf{S}_K$ is symmetric positive definite)

Model refinement
forall $E \in \mathfrak{E}$ **do**
  compute edge refinement indicators η_E using (28)
end
select Kirchhoff elements to be substituted for MR elements based on (29)
introduce new rotational degrees of freedom on selected elements

Combined plate models
forall MR elements $T \in \mathfrak{T}_h$ **do**
  assemble element stiffness matrices $\tilde{\mathbf{S}}_T$ according to (17)
end
forall $E \in \mathfrak{E}_I$ where neighbors T_1 and T_2 are MR elements **do**
  assemble symmetry edge matrices $\tilde{\mathbf{S}}_I^{\text{sym}}$ via (20)
  assemble penalty edge matrix $\tilde{\mathbf{S}}_I^{\text{p}}$ according to (21)
end
forall $E \in \mathfrak{E}_I$ where either T_1 or T_2 is a MR element **do**
  assemble symmetry edge matrices $\mathbf{S}_I^{\text{sym}}$ by (24)
  assemble penalty edge matrix $\mathbf{S}_I^{\text{p}}$ using (25)
end
forall $E \in \mathfrak{E}_B$ where T is a MR element **do**
  assemble symmetry edge matrices $\tilde{\mathbf{S}}_B^{\text{sym}}$ via (20)
  assemble penalty edge matrix $\tilde{\mathbf{S}}_B^{\text{p}}$ according to (21)
end
construct sparse stiffness matrix $\mathbf{S}_C$ (reuse previous assembly data) and pad $\mathbf{f}_C$ with zeros
solve linear system $\omega = \mathbf{S}_C^{-1}\mathbf{f}_C$ (use that $\mathbf{S}_C$ is symmetric positive definite)

subjected to the transverse surface load

$$f = \frac{E}{12(1-\nu^2)}\big(12x_2(x_2-1)(5x_1^2-5x_1+1)(2x_2^2(x_2-1)^2+x_1(x_1-1)(5x_2^2-5x_2+1)+ \\ 12x_1(x_1-1)(5x_2^2-5x_2+1)(2x_1^2(x_1-1)^2+x_2(x_2-1)(5x_1^2-5x_1+1)\big).$$

The exact solution of the MR formulation (2) for this plate problem was stated by Chinosi *et. al.* [7],

$$u(x_1,x_2) = \tfrac{1}{3}x_1^3(x_1-1)^3x_2^3(x_2-1)^3 - \frac{2t^2}{5(1-\nu)}\big(x_2^3(x_2-1)^3x_1(x_1-1)(5x_1^2-5x_1+1)+ \\ x_1^3(x_1-1)^3x_2(x_2-1)(5x_2^2-5x_2+1)\big),$$

and

$$\boldsymbol{\theta}(x_1,x_2) = \begin{bmatrix} x_2^3(x_2-1)^3x_1^2(x_1-1)^2(2x_1-1) & x_1^3(x_1-1)^3x_2^2(x_2-1)^2(2x_2-1) \end{bmatrix}^{\mathrm{T}}.$$

Let $E = 1$, $\nu = 1/3$, and set $\gamma = 10k^2 = 40$ (sufficiently large by a margin). The computational mesh, as shown in Figure 1, is dense in order to emphasize the modeling error. $\mathfrak{T}_h$ is of criss-cross type, which is a mesh less sensitive to locking for low-order approximations due to large stabilization parameters, see [4, Section 4.2] and [3, Section 7.2]. The homogeneous Dirichlet boundary condition on the displacements is set strongly, whereas the condition is enforced weakly on the rotation vector (but this is rather a matter of choice).

The problem was solved numerically for different plate thicknesses, ranging from $t = 10^{-1}$ to $t = 10^{-4}$. The results are presented in Table 1, and indicate the relative importance of model refinement for thicker plates. The underlying combined models, which are independent of the plate thickness, are shown in Figure 3. The distributions of MR elements were symmetric, as is the analytical displacement solution, visualized by isolines in Figure 2.

6 CONCLUSIONS

The introduced method for combing the Kirchhoff and MR plate models has a drawback: the number of degrees of freedom becomes larger, as compared to a purely continuous method. Hence the suggested approach may not be computationally competitive (at least not if the number of MR elements is large). However, its real strength is another—the c/dG FEM is simple and straightforward to implement: it is relatively easy to change the order d of the polynomial approximation (especially if the approximating space for the rotation vector is spanned by the corresponding set of monomials). In particular, there is no need for projections of the rotation vector in the shear energy functional.

The suggested c/dG FEM appears to be a viable choice in the context of model adaptivity for plate theory. As for the (small) hierarchy comprising the Kirchhoff and Mindlin-Reissner plate models, it still remains to develop reliable *a posteriori* error estimates, which separate the discretization and modeling errors.

Table 1: *The relative displacement error in global L_2 norm for various plate thicknesses*

ref. ratio r	$t = 10^{-1}$	$t = 10^{-2}$	$t = 10^{-3}$	$t = 10^{-4}$
0.00	$1.182 \cdot 10^{-1}$	$1.664 \cdot 10^{-3}$	$4.008 \cdot 10^{-4}$	$3.887 \cdot 10^{-4}$
0.20	$1.084 \cdot 10^{-1}$	$1.486 \cdot 10^{-3}$	$3.900 \cdot 10^{-4}$	$3.880 \cdot 10^{-4}$
0.40	$9.366 \cdot 10^{-2}$	$1.259 \cdot 10^{-3}$	$3.811 \cdot 10^{-4}$	$3.874 \cdot 10^{-4}$
0.60	$7.611 \cdot 10^{-2}$	$9.529 \cdot 10^{-4}$	$3.697 \cdot 10^{-4}$	$3.868 \cdot 10^{-4}$
0.80	$3.592 \cdot 10^{-2}$	$4.983 \cdot 10^{-4}$	$3.582 \cdot 10^{-4}$	$3.860 \cdot 10^{-4}$
0.90	$1.262 \cdot 10^{-2}$	$2.994 \cdot 10^{-4}$		
0.95	$3.214 \cdot 10^{-3}$	$2.278 \cdot 10^{-4}$		
1.00	$1.836 \cdot 10^{-4}$	$2.113 \cdot 10^{-4}$	$3.489 \cdot 10^{-4}$	$3.851 \cdot 10^{-4}$

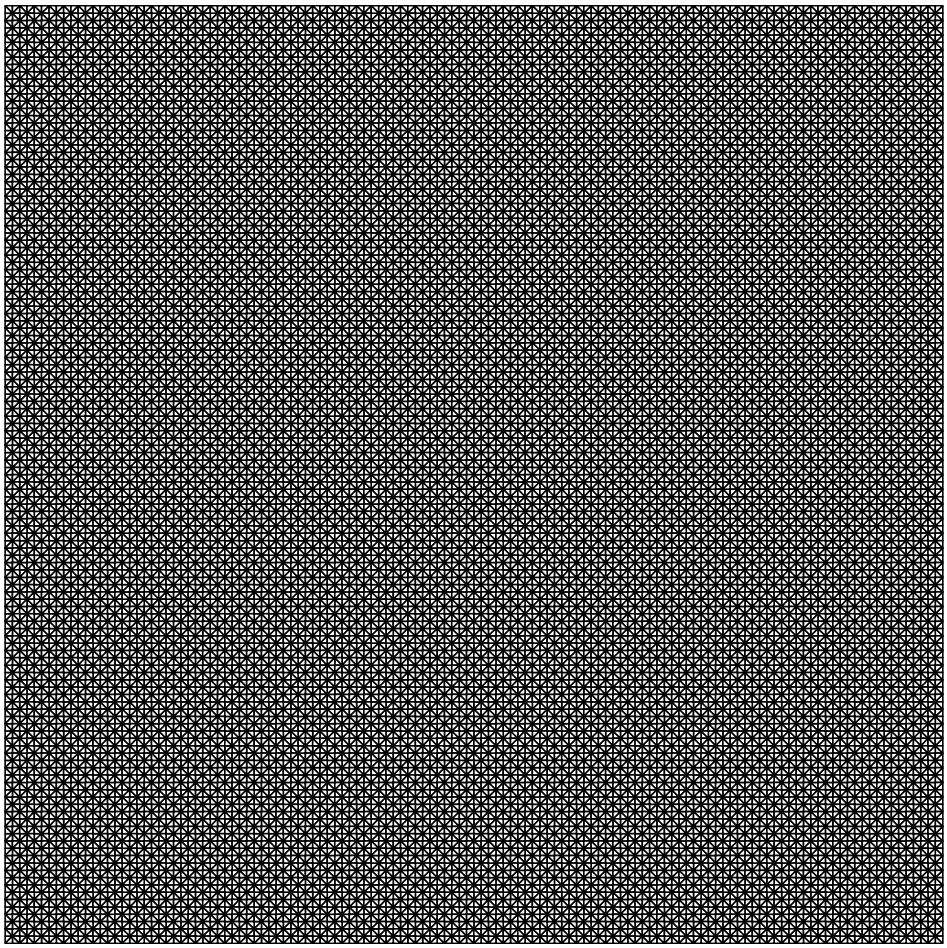

Figure 1: *The triangulation $\mathfrak{T}_h$ of Ω comprised 32 768 elements and 66 049 nodes*

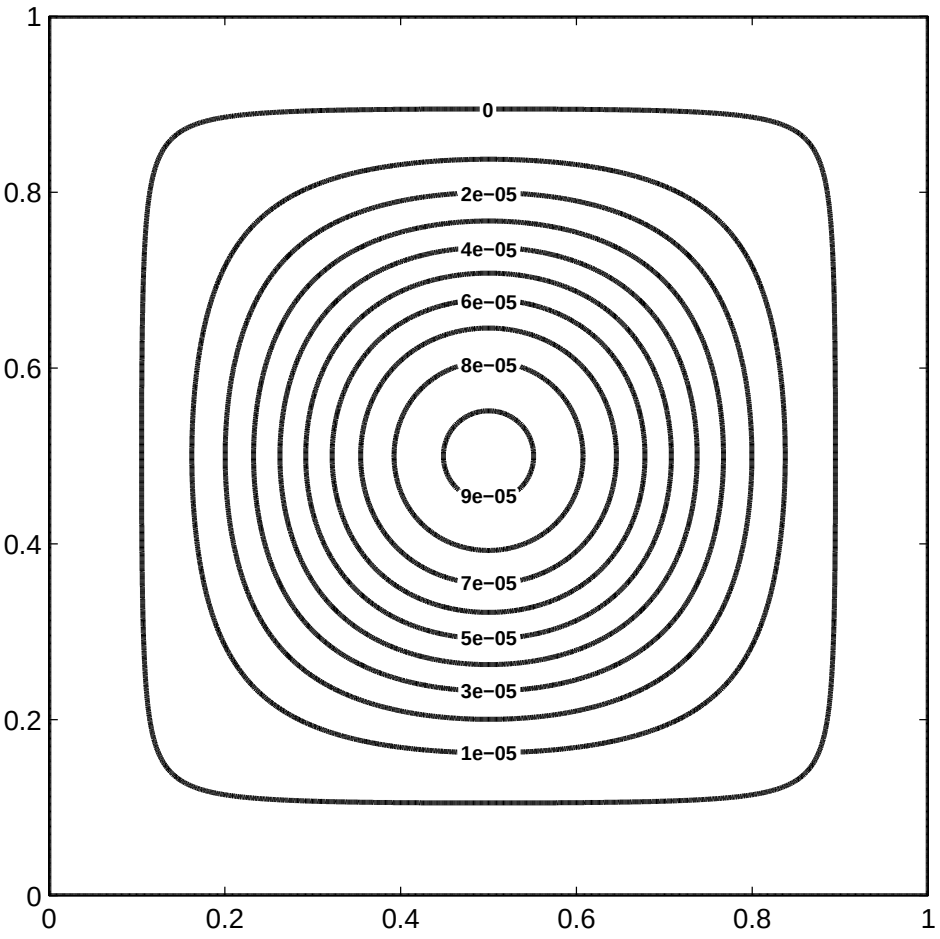

Figure 2: *Transverse displacements (isolines) for the MR plate model with* $t = 10^{-1}$

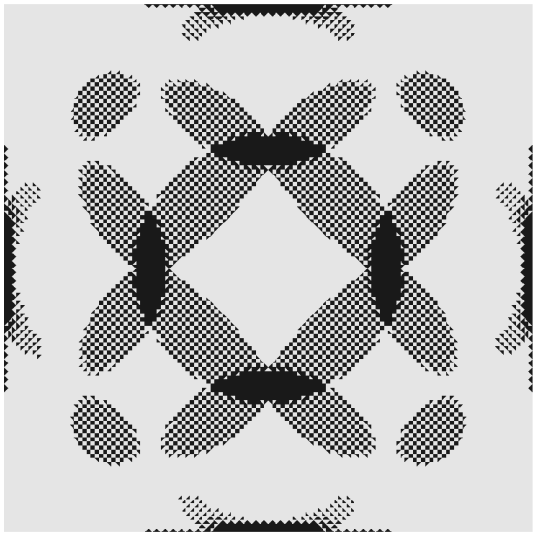

(a) *Refinement ratio* $r = 0.2$

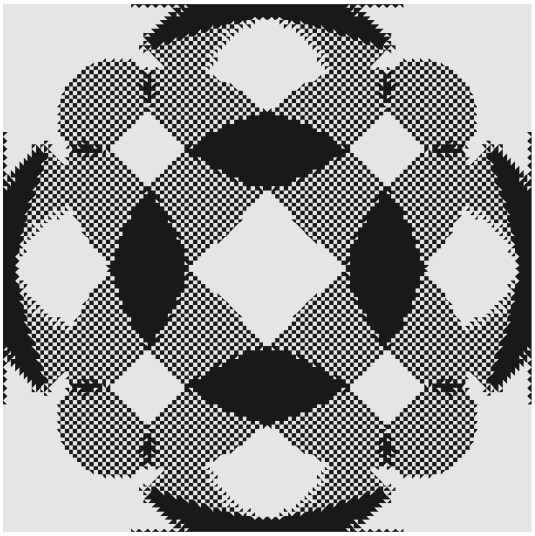

(b) *Refinement ratio* $r = 0.4$

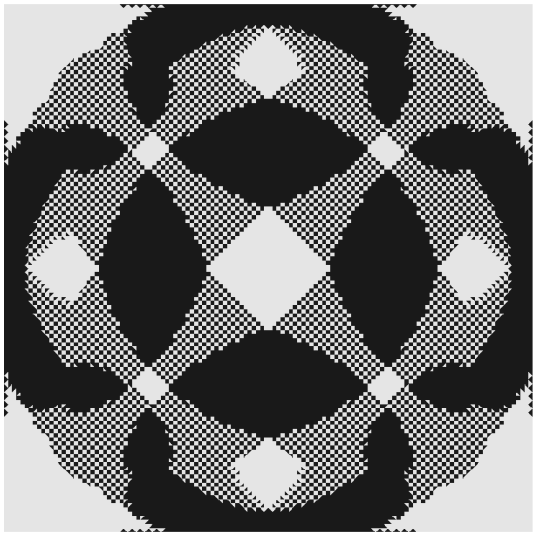

(c) *Refinement ratio* $r = 0.6$

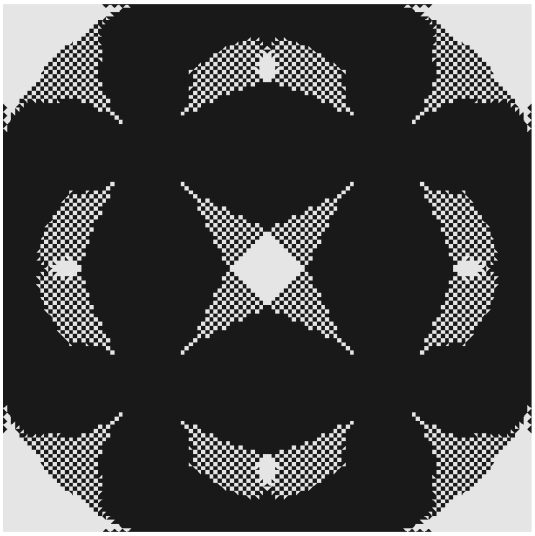

(d) *Refinement ratio* $r = 0.8$

Figure 3: *The underlying combined plate models: distribution of Kirchhoff (light gray) and MR (dark gray) elements*

References

[1] *Engel G, Garikipati K, Hughes TJR, Larson MG, Mazzei L, Taylor RL.* Continuous/discontinuous finite element approximations of fourth-order elliptic problems in structural and continuum mechanics with applications to thin beams and plates, and strain gradient elasticity. *Comput. Methods Appl. Mech. Engrg.* 2002; **191**:3669-3750.

[2] *Hansbo P, Larson MG.* A P^2-continuous, P^1-discontinuous Galerkin method for the Mindlin-Reissner plate model. *Numerical Mathematics and Advanced Applications: ENUMATH 2001*. Brezzi F, Buffa A, Corsaro S, Murli A (Eds.), Springer, Milan, 2003, pp. 765-774.

[3] *Hansbo P, Heintz D, Larson MG.* A finite-element method with discontinuous rotations for the Mindlin-Reissner plate model. *Preprint: Department of Mathematical Sciences, Chalmers University of Technology and Göteborg University*, ISSN 1652-9715, 2010:16.

[4] *Hansbo P, Larson MG.* A posteriori error estimates for continuous/discontinuous Galerkin approximations of the Kirchhoff-Love plate. *Preprint: Department of Mathematical Sciences, Chalmers University of Technology and Göteborg University*, ISSN 1652-9715, 2008:10.

[5] *Hansbo P, Larson MG.* A discontinuous Galerkin method for the plate problem. *Calcolo* 2002; **39**:41-59.

[6] *Nitsche J.* Über ein Variationsprincip zur Lösung von Dirichlet-Problemen bei Verwendung von Teilräumen, die keinen Randbedingungen unterworfen sind. *Abh. Math. Sem. Univ. Hamburg* 1971; **36**:9-15.

[7] *Chinosi C, Lovadina C, Marini LD.* Nonconforming locking-free finite elements for Reissner-Mindlin plates. *Comput. Methods Appl. Mech. Engrg.* 2006; **195**:3448-3460.

[8] *Bathe KJ, Dvorkin EN.* A four-node plate bending element based on Mindlin/Reissner plate theory and a mixed interpolation. *Int. J. Numer. Methods Engrg.* 1985; **21**:367-383.

[9] *Bathe KJ.* Finite Element Procedures. *Prentice-Hall* 1996; ISBN 0-13-301458-4.